Resonance Frequency Tracking for MEMS Gyroscopes Using Recursive Identification

Federico Morelli, Xavier Bombois, Cécile Pernin, Fabricio Saggin, Anton Korniienko, Kévin Colin, Laurent Bako

Resonance Frequency Tracking for MEMS Gyroscopes Using Recursive Identification

F. Morelli, X. Bombois, C. Pernin, F. Saggin, A. Korniienko, K. Colin, L. Bako

***Abstract*— MEMS gyroscopes are generally made up of two resonant systems: the so-called drive and sense modes. It is well known that the tracking of the drive-mode resonance frequency is crucial to make the device operate accurately. In this paper, we propose an approach based on recursive identification that allows to estimate this resonance frequency over the time. The proposed approach pertains to a recently developed control configuration which is based on the H_∞ control framework and allows this configuration to give satisfactory control performance even when the drive-mode resonance frequency changes due to environment effects.**

I. Introduction

In the recent years, micro-electro-mechanical (MEMS) inertial sensors have found their way in our daily life. Indeed, most of the smart phones are equipped with accelerometers and gyroscopes to ensure e.g., image stabilization. The field of application of MEMS inertial sensors is actually much wider. MEMS inertial sensors can indeed also be found in drones and autonomous vehicles, in automotive safety systems, in consumer electronics, in guidance and navigation systems, in numerous industrial applications and in medical devices [18].

In this paper, we are particularly interested in MEMS gyroscopes. A MEMS gyroscope is made up of two proof masses (the so-called drive and sense modes) and allows to determine the angular rate of an object using the Coriolis effect. In order to use this effect, a control system ensures that one of the proof masses (the drive mode) vibrates in a controlled way [16]. Indeed, if the latter is done appropriately, the value of the angular rate can be accurately estimated from a measure of the Coriolis force acting on the second proof mass (the sense mode). For the sequel, it is important to note that MEMS gyroscopes have to operate in a large range of external circumstances. Consequently, the gyroscope performance must be made robust against environment changes. This paper considers this problem and focuses more particularly on the control performance of the drive mode.

As mentioned above, it is of the utmost importance that the proof mass of the drive mode vibrates in a controlled way. This proof mass is fixed to a reference frame via micro-silicon beams and can be driven via an electrostatic force. The transfer function between this force u_x and the position x of the mass can generally be accurately represented by a (lightly-damped) second-order resonating system (an extra pole may be necessary to account for the instrumentation). We will call this system the *drive mass system* in the sequel. This drive mass system must thus vibrate in a controlled way. By this, we mean that x must follow a sinusoidal reference signal x_{ref}. The frequency of the to-be-tracked sinusoidal reference x_{ref} is chosen equal to the resonance frequency of the drive mass system in order to reduce the energy consumption (i.e., to enforce a small actuation signal u_x). Different approaches have been considered in the literature to enforce this objective. A first group of methods is based on the phasor representation of the to-be-controlled signal x. The tracking objective is indeed achieved via two parallel loops that respectively control the amplitude and the phase of this phasor representation (see e.g. [6]). In [2], the amplitude information is used to generate a non-linear oscillator at the resonance frequency. Besides these approaches, the literature also considers techniques that are more classical from a control engineering point-of-view (i.e., adaptive control [7], [8], [11], active disturbance rejection [5], Model Predictive Control [12] and H_∞ control [13], [15]). These techniques compute the control action u_x based on the actual measurement of the position x of the drive mass system (i.e., without having first to transform the signal x into its phasor description). In this paper, we will more particularly consider the H_∞ control configuration introduced in [13], [15] and where the force u_x is computed as the output of a linear time-invariant (LTI) controller K_x that takes as input the difference between the sinusoidal reference signal x_{ref} and the measurement of the position x of the proof mass of the drive mode. As shown in Chapters 3 and 4 of [13], the H_∞ framework allows one to define the specifications of the controller K_x in order to guarantee an accurate measurement of the angular rate by the MEMS gyroscope.

In the drive mass control system, the environmental conditions also play an important role. It is indeed well known [16] that the value of the resonance frequency of the drive mass system is influenced by a number of factors (such as the ambient temperature). In the control configuration considered in [2], [6], these variations of the resonance frequency are relatively easily taken care of. As opposed to this, in the control configuration with a linear controller (the one considered in this paper), it is crucial to be able to adapt the frequency of the sinusoidal reference signal in such a way that this

The financial support of BPI France (Next4MEMS project) is gratefully acknowledged.

The authors are with Laboratoire Ampère, Ecole Centrale de Lyon, Université de Lyon, Ecully, 69134 France (e-mail: federico.morelli.eng@gmail.com; xavier.bombois@ec-lyon.fr; cecile.pernin@ec-lyon.fr; fabricio.saggin@ec-lyon.fr; anton.korniienko@ec-lyon.fr; laurent.bako@ec-lyon.fr).

Xavier Bombois is also with the Centre National de la Recherche Scientifique (CNRS), France.

Kévin Colin is with School of Electrical Engineering and Computer Science, KTH, Stockholm, Sweden (e-mail: kcolin@kth.se).

frequency remains always close to the current value of the resonance frequency of the drive mass system. Otherwise, the amplitude of the control signal u_x will increase, yielding an increase of the energy consumption. This may even lead to the saturation of the actuator and thus to a dramatic loss of performance of the drive mass control system. To prevent this, we propose in this paper an approach to adapt the reference signal x_{ref}. More precisely, we propose an algorithm that estimates the resonance frequency over time. This estimate can then be used to adapt the frequency of the sinusoidal reference signal x_{ref}. The above-mentioned algorithm is based on a recursive identification scheme that allows to follow the evolution of the dynamics of the drive mass system over time and, therefore, also the evolution of its resonance frequency. This approach is here possible since the variation of the resonance frequency of the drive mass system is typically order of magnitude slower than the dynamics of the drive mass system.

The proposed solution relies on the theory of system identification [9] which has already been used to derive nominal models of MEMS gyroscopes (see e.g., [3], [17]). Moreover, in [19], recursive identification is also proposed to follow the evolution of the resonance frequency of systems like the drive mass system. In this interesting paper, however, the drive mass system is not operated in closed loop with a controller K_x and the recursive identification pertains to the estimate of a single parameter linked to the resonance frequency while, in our approach, the whole dynamics of the drive mass system is recursively identified in order to increase the accuracy of the estimate. Finally, unlike in [19], we here also present experimental results to validate the proposed approach.

For this purpose, we have implemented the recursive identification scheme on a test benchmark platform where a development kit designed for experimenting new control strategies for MEMS sensors (the AS3125-SDK platform developed by ASYGN) is used in combination with a MEMS gyroscope prototype (see [15]). Using a thermal chamber to enforce temperature variations (and thus resonance frequency variations), we show that the proposed recursive identification scheme allows to appropriately follow the evolution of the resonance frequency. More importantly, we also show that the performance of the closed loop made up of the drive mass system and of an H_∞ controller K_x is strongly improved when we adapt the frequency of the sinusoidal reference x_{ref} based on this estimate of the resonance frequency (compared to the case where this is not done).

Notations: The matrix I_n denotes the identity matrix of dimension n. The symbol z will not only represent the Z-transform variable, but also the shift operator. For a discrete-time signal $x(t)$, t represents the sample number. Finally, $\mathbb{R}$ denotes the set of real numbers.

II. Description of the drive mass system and of its control system

A. Nominal control design and nominal performance

In Figure 1, we present the H_∞ control strategy that has been proposed for the drive mass system G_x in [13]. This control strategy is implemented in discrete time with a sampling time $T_s = 1.6\ 10^{-5}\ s$. In Figure 1, $x_{ref}(t)$ is the sinusoidal reference signal, u_x is a voltage proportional to the force applied to the drive mass system (i.e., the input of the drive mass system), x is a voltage proportional to the (measured) position of the drive mass[1] and v_x the process and measurement noise acting on the drive mass system. Finally, $K_x(z)$ is the discrete-time H_∞ controller designed based on a nominal model $\hat{G}_x(z)$ of $G_x(z)$. This nominal model $\hat{G}_x(z)$ is here a third-order discrete-time transfer function that has been obtained using the open-loop prediction error procedure presented in Chapter 7 of [3]. It is important to stress that this nominal model will only accurately represent the drive mass system when the factors influencing the resonance frequency will be close to the ones observed during the identification experiment. In our case, the ambient temperature at which the experiment has been performed was $30\ ^oC$.

In Figure 2, we observe that $\hat{G}_x$ is a resonating system that has a significant gain (i.e., 9 dB) only at its resonance frequency $\omega_{r,x} = 72788.728864\ rad/s$ (i.e., 11.5 kHz). Since a resonating system can be better understood in the continuous time, let us consider the following continuous-time version of $\hat{G}_x(z)$:

$$\tilde{G}_x(s) = \frac{k}{(\frac{s^2}{\omega_{n,x}^2} + \frac{2\xi}{\omega_{n,x}}s + 1)(\frac{s}{k_f} + 1)} \tag{1}$$

with s the Laplace variable. In this equation, the resonator is described by its (very low) damping ratio $\xi = 5.9\ 10^{-6}$ and its natural frequency $\omega_{n,x} = 72788.728866\ rad/s$, while $k = -5.46\ 10^{-5}$ is the static gain of the transfer function and the pole $-k_f$ ($k_f = 5.7\ 10^4$) is due to the instrumentation. The resonance frequency of $\tilde{G}_x(s)$ (and of $\hat{G}_x(z)$) is defined as the frequency $\omega_{r,x}$ at which the modulus $|\tilde{G}_x(j\omega)|$ of the frequency response of $\tilde{G}_x$ is the largest i.e., $\omega_{r,x} = 72788.728864\ rad/s$ (i.e., 11.5 kHz). This frequency is extremely close to the natural frequency $\omega_{n,x}$ due to the low damping ratio ξ and can be deduced[2] as $\omega_{r,x} = \omega_{n,x}\sqrt{1-2\xi^2}$. For further reference, the resonance frequency $\omega_{r,x} = 72788.728864\ rad/s$ will be denoted $\omega_{r,x}^{nom}$ since it is the resonance frequency of the nominal model.

The identification procedure in [3] also allows to derive an estimate of the process and measurement noise $v_x(t)$ acting on the system. In particular, v_x can be modeled as a time-series with a standard deviation of 0.0027 V and with a frequency content that is mainly located in the interval

[1] With some abuse, we will not distinguish the actual position and its measurement.

[2] This relation is in fact a (small) approximation since this relation is only valid for a second-order resonator.

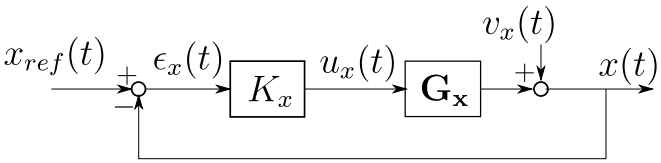

Fig. 1: Schematic of the control strategy of the drive mass system.

$[0\ 100]\ rad/s$. More details on the identification results are given in the appendix.

As already mentioned, the H_∞ controller $K_x(z)$ is determined based on the nominal model $\hat{G}_x(z)$ of $G_x(z)$. Since the magnitude gain of $\hat{G}_x$ is negligible at all frequencies except at the resonance frequency $\omega_{r,x}^{nom}$, the tracking of a sinusoidal reference signal at another frequency than $\omega_{r,x}^{nom}$ would require an overly large control effort. Consequently, we will choose $x_{ref}(t) = A_x \sin\left(\omega_{r,x}^{nom}\ t\ T_s\right)$ with $A_x = 0.5\ V$ the desired amplitude of the oscillation. Given this, the controller K_x is then designed in such a way that the tracking of x_{ref} is accurate enough for the sensing objective of the MEMS gyroscope. As shown in Chapter 3 of [13], the design, based on the nominal model $\hat{G}_x(z)$, of such a controller K_x can be formulated as a convex optimization problem involving an H_∞ criterion [13], [15]. This leads to the fourth-order controller $K_x(z)$ given in the appendix. By observing the high gain characteristic at $\omega = \omega_{r,x}^{nom}$ of both $\hat{G}_x$ and K_x in Figure 2, it is clear that the nominal closed-loop $[K_x\ \hat{G}_x]$ will ensure an accurate tracking of $x_{ref}(t) = A_x \sin\left(\omega_{r,x}^{nom}\ t\ T_s\right)$.

In order to characterize the performance of this nominal loop $[K_x\ \hat{G}_x]$ more precisely, we can simulate it with $x_{ref}(t) = A_x \sin\left(\omega_{r,x}^{nom}\ t\ T_s\right)$ and with a disturbance $v_x(t)$ having a standard deviation of $0.0027\ V$ and the low frequency content evidenced by the identification experiment. This simulation is performed for 70 seconds. During the first four seconds of this simulation, the amplitude A_x of x_{ref} is progressively increased from zero to $0.5\ V$ (in order to limit the transient behaviour). In Figure 3 and Figure 4, we give the obtained control signal $u_x(t)$ and tracking error $\epsilon_x(t) = x_{ref}(t) - x(t)$. Since they are obtained on the closed loop made up of the nominal model $\hat{G}_x(z)$ and of the controller $K_x(z)$ designed with that model, the signals given in Figure 3 and Figure 4 are representative of the desired level of performance (i.e., the *nominal performance*). In particular, an actuation signal u_x of (maximal) amplitude $0.2\ V$ and a tracking error ϵ_x of (maximal) amplitude $0.015\ V$, both including noise, will therefore be seen as *nominal* performance.

B. Time-varying nature of G_x

The control strategy presented above will however not be sufficient to maintain the desired performance. Indeed, due to a number of factors among which temperature variation is the most important, the dynamics of G_x (in particular, its resonance frequency $\omega_{r,x}$) will vary with time. Let us analyze this variation more in details.

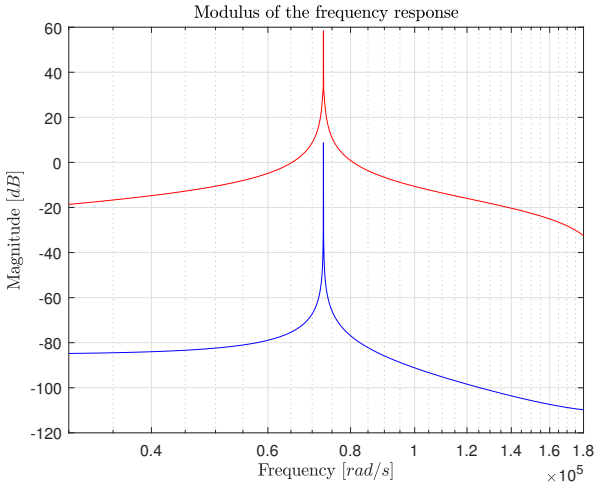

Fig. 2: Modulus of the the frequency response of $\hat{G}_x(z)$ (blue) and of $K_x(z)$ (red).

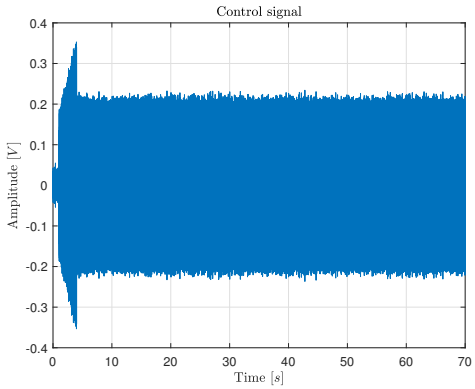

Fig. 3: Signal $u_x(t)$ obtained in the simulation described in Section II.A (nominal performance).

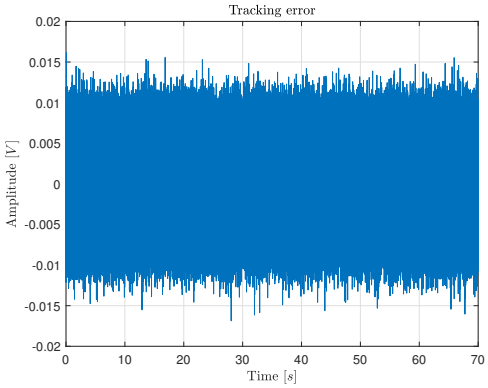

Fig. 4: Signal $\epsilon_x(t)$ obtained in the simulation described in Section II.A (nominal performance).

The gyroscope must function properly for temperatures ranging from -10 ^oC to 70 ^oC and for a rate of temperature variation that is smaller than 0.05 ^oC per second. In steady state, one generally observes that the resonance frequency is decreased by 1 rad/s when the temperature is increased by 1 ^oC. Consequently, the interval in which the resonance frequency $\omega_{r,x}$ will vary is $[72748 \quad 72828]$ rad/s ($\omega_{r,x}^{nom} = 72788$ rad/s indeed corresponds to a temperature of 30 ^oC). Let us first note that the length of this interval is order of magnitude smaller than the value of $\omega_{r,x}$. Moreover, given the maximal rate of temperature variation of 0.05 ^oC per second, it is also clear that the rate at which the resonance frequency $\omega_{r,x}$ will vary in the interval $[72748 \quad 72828]$ rad/s is also order of magnitude slower than the dynamics of the drive mass system (dynamics mainly characterized by $\omega_{r,x}$).

Due to this slow time-varying nature, we will be able to follow the evolution of the dynamics of G_x (and in particular the evolution of its resonance frequency) using recursive identification and this will allow us to make the loop in Figure 1 adaptive. Here, in order to limit the control efforts and the tracking error, we will adapt the frequency of the sinusoidal reference x_{ref} in such a way that it remains at all time as close as possible to the actual resonance frequency of G_x. Indeed, this will ensure that, as in the nominal case, both G_x and K_x will present a significant gain at the frequency of x_{ref}. The gain of K_x remains indeed important in the interval $[72748 \quad 72828]$ rad/s.

Remark. Besides the fact that the gain of K_x remains important in the interval $[72748 \quad 72828]$ rad/s, it can also be proven that K_x stabilizes all transfer functions (1) with a resonance frequency $\omega_{r,x} \in [72748 \quad 72828]$ rad/s. This property coupled with the slow-time varying nature of G_x ensures the validity of the adaptive control scheme presented in the sequel. More details on the robustness of K_x can be found in [1].

III. Recursive estimation of the varying resonance frequency

A. Recursive Identification

Considering the time-varying nature of the drive-mass system (see Section II.B) and considering the fact that the nominal model identified at nominal temperature is a third-order discrete-time transfer function (see the appendix), we can assume the following time-varying model structure for the dynamics of the drive mass system[3]:

$$\begin{cases} \breve{x}(t) = b_{0,1}(t)u_x(t-1) + b_{0,2}(t)u_x(t-2)... \\ \quad ... + b_{0,3}(t)u_x(t-3) - f_{0,1}(t)\breve{x}(t-1)... \\ \quad ... - f_{0,2}(t)\breve{x}(t-2) - f_{0,3}(t)\breve{x}(t-3) \\ x(t) = \breve{x}(t) + v_x(t) \end{cases} \tag{2}$$

[3]The complexity of this model structure can be further reduced by imposing $b_{0,3}(t) = 0$. Indeed, such a model reduction does not influence the accuracy of the estimate of the resonance frequency.

where $\theta_0(t) = (b_{0,1}(t), b_{0,2}(t), b_{0,3}(t), f_{0,1}(t), f_{0,2}(t), f_{0,3}(t))^T$ is the time-varying parameter vector of dimension $n = 6$. Recursive identification is an identification technique that allows to derive models of time-varying systems such as the one given in (2) via the determination at each (discrete) time instant of an estimate $\hat{\theta}(t)$ of its time-varying parameter vector $\theta_0(t)$. From this time-varying model $\hat{G}_x(t)$, we will be able to derive an estimate $\hat{\omega}_{r,x}(t)$ of the resonance frequency $\omega_{r,x}(t)$ (it will then be used to adapt the sinusoidal reference x_{ref} of the closed loop made up of the drive mass system and the controller K_x). As we will see in the sequel, at each sample t, this estimate $\hat{\omega}_{r,x}(t)$ will be given by the resonance frequency of the transfer function that can be obtained if we freeze the coefficients of the time-varying operator $\hat{G}_x(t)$ at their value at sample t.

Note that, unlike in [19], the time-varying model structure (2) does not impose that the resonance frequency is the only parameter that varies over time. It only assumes that the order of the dynamics of the drive mass system will not change over time.

Like in all identification methods, we will need to excite the system with an external signal $r(t)$ in order to guarantee that $\hat{\theta}(t)$ is an accurate estimate of $\theta_0(t)$ (and consequently in order to guarantee that $\hat{\omega}_{r,x}(t)$ is an accurate estimate of $\omega_{r,x}(t)$). This external excitation signal will be denoted $r(t)$ and will be added at the output of the controller K_x (as shown in the bottom of Figure 5):

$$u_x(t) = K_x(z)\left(x_{ref}(t) - x(t)\right) + r(t) \tag{3}$$

In our implementation, in order to ensure the persistence of excitation, $r(t)$ will be chosen as an RBS (Random Binary Sequence) signal of amplitude 0.02 V (which is small with respect to the amplitude of the signal u_x observed in Figure 3). Note that, given the dynamics of G_x, a more narrowband signal $r(t)$ could also have been considered.

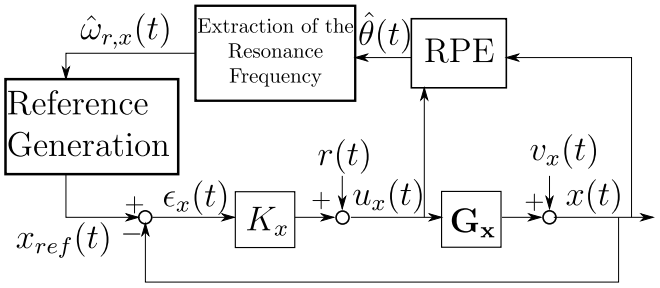

Fig. 5: Control of the drive mass system with the estimate $\hat{\omega}_{r,x}(t)$ of the resonance frequency $\omega_{r,x}(t)$ obtained with the Recursive Prediction Error algorithm.

Let us first present the methodology we have used to determine $\hat{\theta}(t)$ using the measurements of $u_x(t)$ and $x(t)$ obtained in the loop represented in (the bottom of) Figure 5. Among the possible recursive identification algorithms, we had to make a choice that allowed a compromise between the accuracy of the estimate and the numerical complexity (the computational resources available for the algorithm are

indeed limited since the gyroscope is operated with an electronic card). Based on these considerations, we opted for an Output Error (OE) version of a technique called Recursive Prediction Error (RPE) [9]. As such, this OE version neglects the coloring of the process noise $v_x(t)$ and can therefore lead to biased estimates since the identification is performed under closed-loop operation [9]. However, this bias is likely to be small since the identification is here performed under favorable signal-to-noise ratio ($x(t)$ will be of amplitude 0.5 V and $v_x(t)$ has a standard deviation of 0.0027 V). In the RPE algorithm, the estimate $\hat{\theta}(t)$ at sample t is determined by updating the previous value of the estimate, i.e. $\hat{\theta}(t-1)$, using uniquely the output measurement $x(t)$ at sample t and the input measurement $u_x(t-1)$ at sample $t-1$, and using other quantities that are also recursively updated. In particular, we have[4]:

$$\hat{\theta}(t) = \hat{\theta}(t-1) + R^{-1}(t)\ \psi(t)\ \ (x(t) - \hat{x}(t)) \qquad (4)$$

where $x(t)$ is the output measurement at sample t and $R(t) \in \mathbb{R}^{n\times n}$, $\psi(t) \in \mathbb{R}^{n\times 1}$ and $\hat{x}(t) \in \mathbb{R}$ are additional quantities that are recursively determined. The quantities $\hat{x}(t)$ and $\psi(t)$ can be determined using $\hat{\theta}(t-1)$ and the input measurement $u_x(t-1)$ at sample $t-1$ via the following time-varying state-space representation (the state vector $\varphi(t)$ of this state-space representation is thus also recursively updated):

$$\begin{cases} \varphi(t) = \mathcal{A}(\hat{\theta}(t-1))\varphi(t-1) + \mathcal{B}(\hat{\theta}(t-1))u_x(t-1) \\ \begin{pmatrix} \hat{x}(t) \\ \psi(t) \end{pmatrix} = \mathcal{C}(\hat{\theta}(t-1))\ \varphi(t) \end{cases} \qquad (5)$$

where, for any value of $\theta = (b_1, b_2, b_3, f_1, f_2, f_3)^T$, $(\mathcal{A}(\theta),\ \mathcal{B}(\theta), \mathcal{C}(\theta))$ is a state-space representation of the following vector of transfer function[5]:

$$\begin{pmatrix} G(z,\theta) \\ \frac{\partial G(z,\theta)}{\partial \theta} \end{pmatrix} \quad \text{with}$$

$$G(z,\theta) = \frac{b_1 z^{-1} + b_2 z^{-2} + b_3 z^{-3}}{1 + f_1 z^{-1} + f_2 z^{-2} + f_3 z^{-3}} \qquad (6)$$

Finally, the matrix $R(t)$ is determined from $R(t-1)$ using the quantity $\psi(t)$ defined in (5):

$$R(t) = \lambda\ R(t-1)\ +\ \psi(t)\psi^T(t) \qquad (7)$$

where λ is a scalar tuning parameter, the so-called forgetting factor ($0 < \lambda \leq 1$). This parameter is determined by the user based on the assumed rate of variation of $\theta_0(t)$ in order to optimize the bias-variance trade-off of the estimate. In a nutshell, the faster $\theta_0(t)$ varies, the smaller λ has to be chosen. Here, using a trial-and-error approach, we have determined that $\lambda = 1 - 2\ 10^{-5}$ is a reasonable value.

[4]In order to reduce the numerical complexity, the inversion of the matrix $R(t)$ in (4) can be easily circumvented (see e.g., [10, pp. 328]).

[5]It is thus clear that $\hat{x}(t)$ represents the Output Error predictor of $x(t)$ and $\psi(t)$ its gradient.

Once initialized, the recursive algorithm can thus be easily implemented. For this initialization, we have here chosen $\hat{\theta}(0)$ as the parameter vector of the nominal model of the drive mass system i.e., the model identified at nominal temperature and that has been used to design the controller K_x. The other quantities that are recursively updated are initialized as follows $\hat{x}(0) = 0$, $\psi(0) = 0$ and $R(0) = 0.01\ I_n$ (see [10, pp. 299-302] for more details on this choice). Additional features can also be added to the algorithm. It is indeed highly recommended [9, pp. 373] to check at each sample t if the transfer function $G(z,\theta)$ for $\theta = \hat{\theta}(t)$ is stable and, if it is not the case, to replace (4) by $\hat{\theta}(t) = \hat{\theta}(t-1)$. In addition, it may also be wise to regularly re-initialize the recursive algorithm to avoid numerical issues (that can take the form of an estimate $\hat{\theta}(t)$ that remains constant while $\theta_0(t)$ varies).

B. Estimation of the varying resonance frequency using $\hat{\theta}(t)$

Let us now show how we can derive $\hat{\omega}_{r,x}(t)$ from $\hat{\theta}(t)$. If we freeze the value of $\hat{\theta}(t)$ at its value at sample t, the dynamics of the drive mass system can be described by $G(z,\theta^*)$ with $\theta^* = \hat{\theta}(t)$ (see (6)). The estimate $\hat{\omega}_{r,x}(t)$ of $\omega_{r,x}(t)$ at sample t will be then chosen as the resonance frequency of the transfer function $G(z,\theta^*)$. Since the damping of $G(z,\theta^*)$ is very low, we will use the following expression for $\hat{\omega}_{r,x}(t)$:

$$\hat{\omega}_{r,x}(t) = \frac{1}{T_s} \arg(p^*(t)) \qquad (8)$$

where p^* is one of the complex pole of $G(z,\theta^*)$ and $\arg(p)$ denotes the argument of the complex number p. The complex pole of $G(z,\theta^*)$ is here determined in a computationally friendly way via a Newton-Raphson scheme initialized at the complex pole of the initial model.

The estimate $\hat{\omega}_{r,x}(t)$ obtained in this way can then be used to compute $x_{ref}(t)$ as follows:

$$x_{ref}(t) = A_x \sin\left(\sum_{\tau=1}^{t} \hat{\omega}_{r,x}(\tau)\ T_s\right) \qquad (9)$$

As a consequence, the scheme that we propose to tackle the variations of the resonance frequency of the drive mass system (when this system is operated with a linear controller) can be summarized by Figure 5.

Remark. Since the sampling time T_s used by the electronic card is small with respect to the expected variation of the resonance frequency, instead of updating the value of the resonance frequency at each sample t, one could further reduce the numerical complexity by updating the value of $\hat{\omega}_{r,x}(t)$ only every t_w samples i.e., the approach presented in this subsection to derive $\hat{\omega}_{r,x}(t)$ from $\hat{\theta}(t)$ will thus only be required once every t_w samples. This approach is moreover particularly interesting in combination with a recursive algorithm that is frequently re-initialized (see the previous subsection). Indeed, in the instants just after such a re-initialization, the estimate $\hat{\theta}(t)$ of $\theta_0(t)$ may be less

accurate and so would be the estimate $\hat{\omega}_{r,x}(t)$ of $\omega_{r,x}(t)$ that could be deduced from that $\hat{\theta}(t)$. In the implementation of our algorithm, the recursive algorithm will be re-initialized every 30 seconds and the estimate $\hat{\omega}_{r,x}(t)$ of $\omega_{r,x}(t)$ will be determined 15 seconds after each re-initialization[6] and just before the next re-initialization. In other words, the signal $\hat{\omega}_{r,x}(t)$ that will be used to compute x_{ref} will have the form of a staircase signal with a (possible) step every 15 seconds.

IV. Experimental results

In the previous section, we have presented our approach to improve the control of the drive mass system under varying resonance frequency circumstances. The resonance frequency of the drive mass system is estimated through a recursive identification algorithm and this estimate $\hat{\omega}_{r,x}(t)$ is used in the expression (9) of the sinusoidal reference signal $x_{ref}(t)$ (see Figure 5). A MEMS gyroscope prototype has been instrumented with the platform AS3125SDK comprising an electronic card where the H_∞ controller K_x, the recursive identification algorithm and the adaptation of x_{ref} have been implemented in C++. This platform has been chosen for its flexibility and more details can be found at https://asygn.com/as3125-sdk/. The experimental setup is represented in Figure 6.

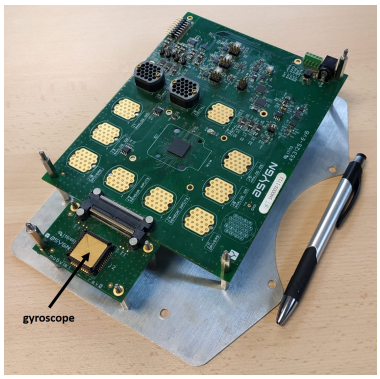

Fig. 6: Picture of the experimental setup with the electronic card AS3125-SDK and the MEMS gyroscope.

Let us recall that the ambient temperature is the most important factor influencing the value of the resonance frequency. Consequently, in order to investigate the performance of our approach, we operated the experimental setup presented in Figure 6 in a thermal chamber. In particular, we imposed a setpoint of 50 ^oC at the start of the experiment and, in response to this setpoint, the temperature measured inside the thermal chamber followed the profile given in Figure 7. In this figure, we observe that the temperature, which is initially equal to 26 ^oC, changes to a temperature of about 52 ^oC in about ten minutes (i.e., a temperature gradient close to the maximal rate of temperature variation of 0.05 $^oC/s$ mentioned in Section II.B). After this, the temperature remains (approximately) constant for another five minutes.

[6]The estimates $\hat{\theta}(t)$ and $\hat{\omega}_{r,x}(t)$ are indeed less accurate only for a few seconds.

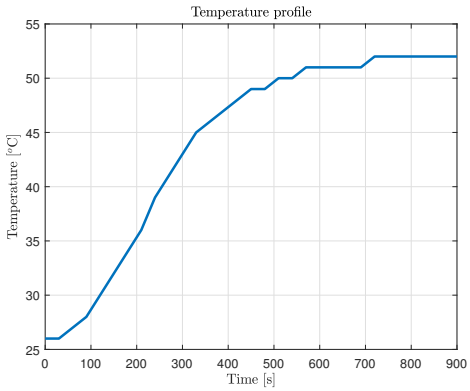

Fig. 7: Temperature profile in the thermal chamber.

Due to the modification of the temperature, the resonance frequency is modified and this fact is confirmed by the estimate $\hat{\omega}_{r,x}(t)$ of this resonance frequency that is computed every 15 seconds by the algorithm described in Section III. This estimate is represented in Figure 8 and is compared to the resonance frequency $\omega_{r,x}^{nom}$ of the nominal model. We observe that, starting at[7] $\omega_{r,x}^{nom}$, the estimation algorithm requires approximately 45 seconds to settle. As we will see in the sequel, from that moment onwards, the control loop (see Figure 5) will have signals u_x and ϵ_x whose amplitudes are very close to the ones observed in Figures 3 and 4 (the so-called nominal performance that we want to maintain). Consequently, the estimate $\hat{\omega}_{r,x}(t)$ can be deemed close to the actual resonance frequency $\omega_{r,x}(t)$ of the drive mass system. Comparing the temperature profile of Figure 7 and the resonance frequency profile of Figure 8, it is clear that the dynamics of the dependence of the resonance frequency on the temperature is rather complex. Let us e.g. observe that $\hat{\omega}_{r,x}(t)$ stays around 72786 rad/s during a long interval of time while, during the same interval of time, the temperature varies from 26 ^oC to 50 ^oC. The frequency 72786 rad/s is the resonance frequency that corresponds to a *steady-state* temperature of approximately 32 ^oC. However, since the temperature is continuously varying in this interval of time, we never reach steady-state. Note also that, as mentioned in Section II.B, the rate at which the resonance frequency varies in Figure 8 is indeed order of magnitude slower than the dynamics of the drive mass system.

The estimate $\hat{\omega}_{r,x}(t)$ of Figure 8 is used to compute the sinusoidal reference signal x_{ref} via (9). Let us now see how the loop in Figure 5 behaves by inspecting the control signal $u_x(t)$ and the tracking error signal $\epsilon_x(t)$. These signals are represented in red in Figures 9 and 10. During the 45 first seconds where x_{ref} is computed with a less accurate estimate of the resonance frequency (since the estimation algorithm is in its settling phase), we observe a large control effort[8] and a large tracking error confirming the need of constructing x_{ref}

[7]Recall that the recursive identification algorithm is initialized at the nominal model.

[8]The control effort in fact hits the saturation during approximately 30 seconds.

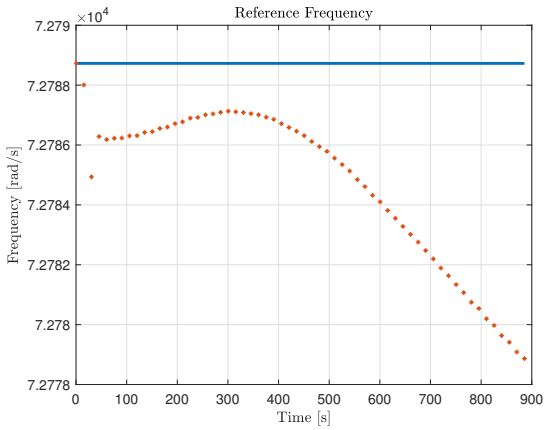

Fig. 8: Estimate $\hat{\omega}_{r,x}(t)$ of the resonance frequency of the drive mass system (red asterisks) compared to the resonance frequency $\omega_{r,x}^{nom}$ of the nominal model (blue solid line).

with a good estimate of the resonance frequency. After this settling phase, the signals $u_x(t)$ and $\epsilon_x(t)$ present amplitudes that are very close to the ones observed in the nominal case (see Figures 3 and 4). Note that we observe a very small increase of the amplitude of u_x in the second part of the experiment. This may be due to the combination of, on the one hand, the faster decrease of the resonance frequency in this part of the experiment (see Figure 8) and, on the other hand, the fact that $\hat{\omega}_{r,x}(t)$ is only updated every 15 seconds (see the remark at the end of Section III).

As already mentioned, the differences between the settling phase (where $\hat{\omega}_{r,x}(t)$ is less accurate) and the remaining of the red curves presented in Figures 9 and 10 clearly show the efficiency of our approach to deal with the adverse consequences of the variations of the resonance frequency when the drive mass system is controlled using the LTI controller K_x. In order to illustrate the benefit of our approach even further, let us perform a similar experiment in the thermal chamber without the adaptation of the reference signal x_{ref} i.e., x_{ref} is kept during the whole experiment equal to $x_{ref}(t) = 0.5\sin(\omega_{r,x}^{nom} t T_s)$ i.e., a sinusoid at the resonance frequency $\omega_{r,x}^{nom}$ of the nominal model. This leads to the signals u_x and ϵ_x given in blue in Figures 9 and 11. By comparing the blue and red curves in Figure 9, it is clear that the control signal $u_x(t)$ is much larger when $x_{ref}(t) = 0.5\sin(\omega_{r,x}^{nom} t T_s)$ than when x_{ref} is adapted. This is particularly obvious in the second part of the experiment where the variation of the resonance frequency is stronger (see Figure 8) and where u_x hits its saturation. This saturation of the control effort has a dramatic effect on the tracking error whose amplitude becomes almost as large as x_{ref} (see Figure 11). Comparing the blue and red curves in Figures 9 and 11 clearly evidences the necessity of adapting x_{ref} to tackle the variations of the resonance frequency when the drive mass system is controlled using a LTI controller.

The proposed algorithm is of course also useful when the change of the ambient temperature is less important. Indeed, as the controller is designed for a given nominal model, even small variations near these nominal conditions can deteriorate the performances due to small resonance frequency variations. We have also made multiple tests in these conditions with similar results i.e., signals $u_x(t)$ and $\epsilon_x(t)$ presenting amplitudes that are very close to the ones observed in the nominal case. Since no thermal chamber has to be used for these tests, we have also been able to subject the setup to different rotational speeds using a turning table. We have tested rotational speeds ranging from -300 till 300 degrees per second and the signals $u_x(t)$ and $\epsilon_x(t)$ presented amplitudes that were also very close to the ones observed in the nominal case.

Remark. When facing resonance frequency variations that can be as important as the ones in Figure 8, the adaptation of x_{ref} proposed in this paper allows to maintain the (maximal) amplitudes of u_x and ϵ_x close to the ones observed in the nominal case (see Figures 3 and 4). Consequently, in order to tackle such resonance frequency variations, there seems to be no need of a more complex approach which, besides the adaptation of x_{ref}, would also involve the adaptation of K_x. If this would happen to be necessary in certain situations, let us however note that our recursive identification scheme would also enable the adaptation of K_x. The estimate $\hat{\theta}(t)$ could indeed be used as scheduling parameter in a Linear Parameter Varying controller (see e.g., [4]). Alternatively, as proposed in [14], one could also just use $\hat{\omega}_{r,x}(t)$ as scheduling parameter.

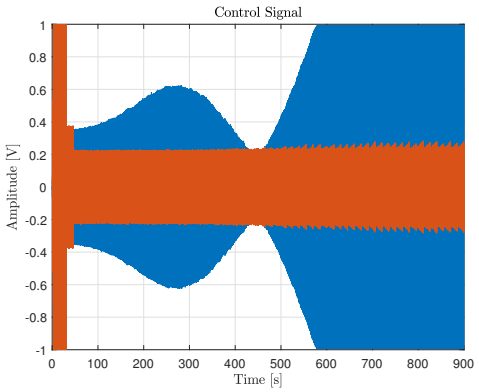

Fig. 9: Results of the experiment in Section IV: $u_x(t)$ when $x_{ref}(t) = 0.5\sin(\omega_{r,x}^{nom} t T_s)$ (blue) and $u_x(t)$ when $x_{ref}(t)$ is adapted as shown in Figure 5 (red).

V. Conclusion

In a MEMS gyroscope, the proof mass of the drive mode (i.e., the drive mass system) must oscillate at its resonance frequency. When using a linear time-invariant controller to generate this oscillation, the variations of the resonance frequency (due e.g., to temperature variations) can severely alter the performance of the MEMS gyroscope. In this paper, we use recursive identification to estimate the dynamics of the drive mass system over time. Using this dynamics, we derive an estimate of the resonance frequency that is

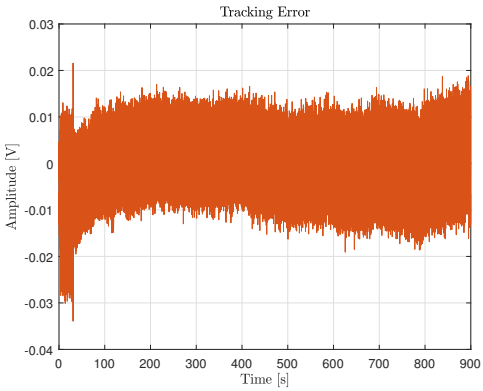

Fig. 10: Results of the experiment in Section IV: $\epsilon_x(t)$ when $x_{ref}(t)$ is adapted as shown in Figure 5 (red).

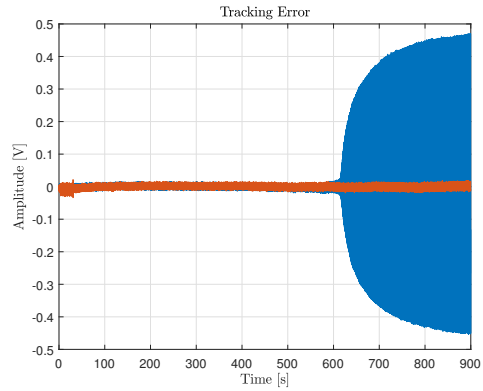

Fig. 11: Results of the experiment in Section IV: $\epsilon_x(t)$ when $x_{ref}(t) = 0.5\sin(\omega_{r,x}^{nom} t T_s)$ (blue) and $\epsilon_x(t)$ of Figure 10 (red).

used to adapt the frequency of the sinusoidal reference signal that must be followed by the drive mass system. The experimental results show that the proposed approach allows to maintain a performance level that is very close to the nominal performance level. By performance, we here mean the amplitudes of the tracking error and of the control actuation.

REFERENCES

[1] J. Ayala. *Performance validation of MEMS Gyroscopes using Uncertain and Time-Varying Models* PhD thesis, Ecole Centrale de Lyon, Université de Lyon, 2021. Available at https://bibli.ec-lyon.fr/exl-doc/TH_T2804_jayala.pdf.

[2] Y-C Chen, R.T. M'Closkey, T.A. Tran, and B. Blaes. A control and signal processing integrated circuit for the JPL-boeing micromachined gyroscope. *IEEE Transactions on Control Systems Technology*, 13(2):286–300, 2005.

[3] K. Colin. *Data informativity for the Prediction Error Identification of MIMO Systems. Identification of a MEMS gyroscope.* PhD thesis, Ecole Centrale de Lyon, Université de Lyon, 2020. Available at https://tel.archives-ouvertes.fr/tel-03114994.

[4] M. Dinh, G. Scorletti, V. Fromion, and E. Magarotto. Parameter dependent H_∞ control by finite dimensional LMI optimization. *Int. J. Robust Nonlinear Control*, 15:383–406, 2005.

[5] L. Dong and D. Avanesian. Drive-mode control for vibrational MEMS gyroscopes. *IEEE transactions on industrial electronics*, 56(4):956–963, 2008.

[6] M. Egretzberger, F. Mair, and A. Kugi. Model-based control concepts for vibratory MEMS gyroscopes. *Mechatronics*, 22(3):241–250, 2012.

[7] J. Fei and C. Batur. Robust adaptive control for a MEMS vibratory gyroscope. *The International Journal of Advanced Manufacturing Technology*, 42(3):293–300, 2009.

[8] R. Leland. Adaptive control of a MEMS gyroscope using lyapunov methods. *IEEE Transactions on Control Systems Technology*, 14(2):278–283, 2006.

[9] L Ljung. *System Identification-Theory for the User 2nd edition, Prentice-Hall*. Upper Saddle River, USA, 1999.

[10] Lennart Ljung and Torsten Söderström. *Theory and practice of recursive identification*. MIT press, 1983.

[11] S. Park, R. Horowitz, S. Hong, and Y. Nam. Trajectory-switching algorithm for a MEMS gyroscope. *IEEE Transactions on Instrumentation and Measurement*, 56(6):2561–2569, 2007.

[12] M. Pishrobat and J. Keighobadi. Model predictive control of MEMS vibratory gyroscope. *IFAC Proceedings Volumes*, 47(3):7278–7283, 2014.

[13] F. Saggin. *Robust control for MEMS gyroscopes*. PhD thesis, Ecole Centrale de Lyon, Université de Lyon, 2021. Available at https://hal.archives-ouvertes.fr/tel-03363650.

[14] F. Saggin, J. Ayala-Cuevas, A. Korniienko, and G. Scorletti. Parameter-dependent H_∞ control for MEMS gyroscopes: synthesis and analysis. *IFAC-PapersOnLine*, 53(2):7331–7337, 2020.

[15] F. Saggin, C. Pernin, A. Korniienko, G. Scorletti, and C. Le Blanc. Digital control of MEMS gyroscopes: a robust approach. In *2021 IEEE International Symposium on Inertial Sensors and Systems (INERTIAL)*, pages 1–4. IEEE, 2021.

[16] M. Saukoski. *System and circuit design for a capacitive MEMS gyroscope*. PhD thesis, Helsinki University of Technology, Faculty of Electronics, Communications and Automation, 2008.

[17] S. Schein and R. M'Closkey. Parametric Model Identification of Axisymmetric MEMS Resonators *Journal of Microelectromechanical Systems*, 2021

[18] D. Shaeffer. MEMS inertial sensors: a tutorial overview. *IEEE Communications Magazine*, 51(4):100–109, 2013.

[19] T. Vasileiou. Model-based resonance tracking of linear systems. *IEEE Transactions on Control Systems Technology*, 2020.

APPENDIX

The identified plant transfer function model $\hat{G}_x(z)$ is given by $\hat{G}_x(z) = (b_1 z^{-1} + b_2 z^{-2} + b_3 z^{-3})/(1 + f_1 z^{-1} + f_2 z^{-2} + f_3 z^{-3})$ with $b_1 = -8.5077647181912\ 10^{-6}$, $b_2 = -2.57566017166506\ 10^{-5}$, $b_3 = -5.4388129619779\ 10^{-6}$, $f_1 = -1.189035255700542$, $f_2 = 1.315148082796523$ and $f_3 = -0.398835278691147$. Moreover, the identification procedure delivers an estimate of v_x given by $\hat{H}_x(z)e_x(t)$ with a white noise e_x of variance $\sigma_e^2 = 2.97\ 10^{-6}$ and with: $\hat{H}_x(z) = (1 + c_1 z^{-1} + c_2 z^{-2} + c_3 z^{-3} + c_4 z^{-4})(1 + d_1 z^{-1} + d_2 z^{-2} + d_3 z^{-3} + d_4 z^{-4} + d_5 z^{-5})$ with $c_1 = 0.9636$, $c_2 = -0.3466$, $c_3 = -1.197$, $c_4 = -0.3669$, $d_1 = -0.05898$, $d_2 = -0.8191$, $d_3 = -0.5455$, $d_4 = 0.5646$ and $d_5 = -0.1345$.

The H_∞ controller $K_x(z)$ is given by $K_x(z) = (g_0 + g_1 z^{-1} + g_2 z^{-2} + g_3 z^{-3} + g_4 z^{-4})/(1 + h_1 z^{-1} + h_2 z^{-2} + h_3 z^{-3} + h_4 z^{-4})$ with $g_0 = 0.124465065398275$, $g_1 = -0.098341705374376$, $g_2 = -3.8803035841\ 10^{-5}$, $g_3 = 0.098336413076116$, $g_4 = -0.124431554660694$, $h_1 = -1.578293401654294$, $h_2 = 2.617438511677789$, $h_3 = -1.574095213951813$ and $h_4 = 0.994687182715191$.